Multiple tidal disruption flares in the active galaxy IC 3599

S. Campana[1], D. Mainetti[1,2], M. Colpi[2], G. Lodato[3], P. D'Avanzo,[1], P. A. Evans[4], A. Moretti[1]

[1] INAF, Osservatorio Astronomico di Brera, Via E. Bianchi 46, 23807, Merate (Lc), Italy
    e-mail: sergio.campana@brera.inaf.it
[2] Dipartimento di Fisica G. Occhialini, Università degli Studi di Milano Bicocca, Piazza della Scienza 3, I-20126 Milano, Italy
[3] Dipartimento di Fisica, Università degli Studi di Milano, Via Celoria 16, I-20133 Milano, Italy
[4] Department of Physics and Astronomy, University of Leicester, University Road, Leicester LE1 7RH, UK

ABSTRACT

Tidal disruption events occur when a star passes too close to a massive black hole and it is totally ripped apart by tidal forces. It may also happen that the star is not close enough to the black hole to be totally disrupted and a less dramatic event might happen. If the stellar orbit is bound and highly eccentric, just like some stars in the centre of our own Galaxy, repeated flares should occur. When the star approaches the black hole tidal radius at periastron, matter might be stripped resulting in lower intensity outbursts recurring once every orbital period. We report on *Swift* observations of a recent bright flare from the galaxy IC 3599 hosting a middle-weight black hole, where a possible tidal disruption event was observed in the early 1990s. By light curve modelling and spectral fitting we can consistently account for the events as the non-disruptive tidal stripping of a star into a highly eccentric orbit. The recurrence time is 9.5 yr. IC 3599 is also known to host a low-luminosity active galactic nucleus. Tidal stripping from this star over several orbital passages might be able to spoon-feed also this activity.

Key words. galaxies: individual: IC 3599 – accretion – X-rays: galaxies – galaxies: active

1. Introduction

Supermassive black holes reside at the centre of most galaxies. When accreting matter, these black holes emit a huge amount of energy, becoming active galactic nuclei (AGNs). The energy and radiation produced by matter accretion onto these black holes play an important role in determining their masses and spins as well as the properties of the host galaxy bulges. AGNs usually have a relatively short duty cycle and are in a low-luminosity state for most of the time (Ho 2008). AGNs may become bright when major inflows of gas feed the compact object (Hopkins et al. 2006). Apart from intense episodes of accretion, the black hole is powered at a floor minimum level mostly by a hot gas from colliding stellar winds in the central region. A star in the nuclear cluster can be scattered close to the black hole via dynamical encounters and put into an orbit too close to the black hole. When the black hole tidal force overcomes the star self gravity (at the so called tidal radius) the star starts to be ripped apart. About half of the star mass remains bound to the black hole, forming an accretion disc and powering a luminous, long lasting (months to years) accretion flare (e.g. Rees 1998; Phinney 1989). Despite their elusiveness, a number of events have been reported in the literature, resulting in the complete disruption of the star (e.g. Renzini et al. 1995; Bloom et al. 2011; Gezari et al. 2012).

Tidal disruption events (TDEs) provide an unique probe to reveal the presence of otherwise quiescent black holes, allowing us to study the accretion process also in a different regime than that of AGNs (Komossa 2012; Gezari 2012). TDEs were first predicted and later on observed in the soft X–ray to ultraviolet bands where the peak of the accretion disc emission lies (Strubbe & Quataert 2009). Two relativistic TDEs were discovered based on high energy triggers, thanks to the launching of relativistic jets along the line of sight (Bloom et al. 2011; Burrows et al.

2011; Cenko et al. 2012). Only a small number of TDEs however have been observed to date in X–ray, UV and optical surveys, mainly because of their low rate of occurrence and sparse observations (Donley et al. 2002).

TDEs are ultimate events. A star entering the tidal radius $r_t \sim R_* (M_{BH}/M_*)^{1/3}$ (where M_{BH} is the black hole mass and M_* and R_* are the mass and radius of the star) is completely disrupted by tidal forces. The fate of a star orbiting its central black hole is then defined by its pericenter radius, r_p: if $\beta = r_t/r_p \gtrsim 1$ we have a TDE. What happens instead if $\beta \lesssim 1$? If β is still close to unity, the star should still feel the black hole tidal force but will survive the encounter. Hydrodynamical simulations show that if the passage is close ($0.5 \lesssim \beta \lesssim 1$) the star may lose matter that can then accrete onto the black hole (Guillochon & Ramirez Ruiz 2013). These events should be more frequent than classical TDEs (roughly by a factor of ~ 10) and should repeat on the star orbital period (if the star is on a bound orbit), increasing their observability. On the other side, these events are less energetic, because the involved mass captured by the black hole is lower.

Here, after a brief introduction on total and partial tidal disruption events (Section 2), we consider the case of a nearby low-luminosity AGN, IC 3599, that showed in the past strong X–ray activity, possibly resulting from a TDE (Brandt, Pounds & Fink 1995; Grupe et al. 1995, see Section 3). In Section 4 we describe new *Swift*/XRT data showing a second, large increase in flux, together with the analysis of all X–ray data on the source. X–ray spectral analysis is presented in Section 5. Based on spectral results, we converted count rates into a flux and then in luminosity. The fit of the overall, 24 yr long, X–ray light curve is described in Section 6. Optical data are discussed in Section 7. In Section 8 we apply partial TDE modelling to the light curve of IC 3599 trying to constrain the involved star and its orbit. Our conclusions are in Section 9.

2. Tidal stripping essentials

A star orbiting too close to a massive black hole will be torn apart by the compact object tidal force. This occurs at the tidal radius beyond which stellar self-gravity is not able to counteract the black hole tidal field and keep the star together. The tidal radius is defined as

$$r_{\rm t} \sim R_* \, (M_{\rm BH}/M_*)^{1/3} \sim 23 \, (M_\bullet^{\rm IC})^{-2/3} \, r_{\rm g}$$

where R_* and M_* are the radius and mass of the star, $M_{\rm BH}$ the mass of the black hole and $M_\bullet^{\rm IC} \sim 3 \times 10^6 M_\odot$ the mass of the central black hole in IC 3599 (Grupe, Komossa & Saxton 2015, see also below). The numerical value refers to a $1 M_\odot$ and $1 R_\odot$ star and units are gravitational radii ($r_{\rm g}$).

As the star is ripped apart by the tidal forces of the black hole, the debris is thrown into high-eccentricity orbits with a large range of periods and with an energy range of (Lacy, Townes & Hollenbach 1982):

$$\Delta E \sim \frac{G \, M_{\rm BH} \, R_*}{r_{\rm t}^2}$$

The distribution of mass as a function of energy is nearly constant (Rees 1988), as also shown by numerical simulations (Evans & Kochanek 1989; Lodato, King & Pringle 2009).

For a parabolic orbit, nearly half of the debris is unbound leaving the system at high velocity. The other half will return to the black hole at different times depending on the initial eccentricity (i.e. energy). The return time of the first debris at pericentre is

$$t_{\rm min} = \frac{2 \pi \, G \, M_{\rm BH}}{(2 \, \Delta E)^{3/2}} \sim \frac{2 \pi \, r_{\rm t}^3}{(G \, M_{\rm BH})^{1/2} \, (2 \, R_*)^{3/2}} =$$
$$= 71 \, R_*^{3/2} \, M_*^{-1} \, (M_\bullet^{\rm IC})^{1/2} \; {\rm d}$$

The return of material at pericentre continues at a rate driven by Kepler's third law as

$$\dot{M} \sim \frac{1}{3} \, \frac{M_*}{t_{\rm min}} \left(\frac{t}{t_{\rm min}} \right)^{-5/3}$$

where the maximum mass inflow rate is

$$\dot{M}_{\rm peak} = \frac{1}{3} \, \frac{M_*}{t_{\rm min}} \sim 1.7 \, R_*^{-3/2} \, M_*^2 \, (M_\bullet^{\rm IC})^{-1/2} M_\odot {\rm yr}^{-1}$$

The peak rate is a function of the stellar structure (Lodato et al. 2009). After disruption, the stellar debris are launched into very eccentric orbits and gradually return to pericentre, where they circularise and form an accretion disc at $r_{\rm circ} \sim 2 \, r_{\rm p}$. The following fall back of this material onto the black hole is governed by viscous times. If the viscous time is short in comparison with $t_{\rm min}$, then the fall back of matter onto the central object is almost instantaneous and $t_{\rm fb} \sim t_{\rm min}$. Based on an $\alpha-$ viscosity disc prescription we can evaluate the viscous time-scale t_ν

$$t_\nu = \frac{t_{\rm Kep}(2 \, r_{\rm p})}{\pi \, \alpha \, h^2}$$

where $t_{\rm Kep}$ is the Keplerian time at a given radius and h is the disc half-height divided by the radius. Being the initial luminosity close to (or even somewhat larger than) the Eddington limit, the disc is expected to be thick (Ulmer 1999), with $h \sim 1$. Thus, we can estimate the ratio of the viscous time to the $t_{\rm min}$ time as

$$\frac{t_\nu}{t_{\rm min}} \sim 1.8 \times 10^{-3} \beta^{-3/2} \left(\frac{\alpha}{10^{-1}} \right)^{-1} (M_\bullet^{\rm IC})^{-1/2} M_*^{1/2} h^{-2}$$

and a thick disc will form and drain as the material circularises down to the last stable orbit.

The infalling star is usually assumed to be in a parabolic orbit and to undergo complete tidal disruption. Encounters may still happen with the pericentre slightly outside the tidal radius ($\beta \lesssim 1$), resulting in some spill over of stellar matter, and orbits can be bound and highly eccentric, resulting in periodic outbursts. This problem received less attention than the classical TDEs but still a number of works exist (Guillochon & Ramirez Ruiz 2013; Macleod, Guillochon & Ramirez-Ruiz 2012; Macleod et al. 2013; Hayasaki, Stone & Loeb 2013; Ivanov & Novikov 2001). If the orbit is bounded the physics is similar to the parabolic case in terms of the effects of black hole tides on the approaching star, especially if the eccentricity is high. On the long term the star orbit may change but the typical orbital binding energy is larger than the stellar binding energy and the orbital angular momentum is larger than the rotational angular momentum of the star, indicating that the transfer of mass will not substantially alter the orbit (Macleod et al. 2013).

In particular, Guillochon & Ramirez Ruiz (2013) investigated the fate of a star undergoing partial stellar stripping. They considered the case of stellar polytropes of $\gamma = 4/3$ and $\gamma = 5/3$ and investigated the case for β within the interval 0.6–4.0 and 0.5–2.5, respectively. They found that total disruption occurs for a critical impact parameter different from unity, being $\beta_c = 1.85$ for $\gamma = 4/3$ and $\beta_c = 0.90$ for $\gamma = 5/3$, respectively. They also provided fitting formulae for estimating the mass accretion peak rate, the peak time, and the total mass transferred for both cases, which are strong functions of β, especially for $\beta \lesssim \beta_c$ (see also the related errata corrige at http://astrocrash.net/2013/09/16/errata-of-guillochon-ramirez-ruiz-2013/). We used these formulae in deriving stellar parameters.

3. IC 3599

One of the first putative TDEs occurred in the close active galaxy IC 3599 (92 Mpc, at a redshift of $z = 0.021$; Brandt et al. 1995; Grupe et al. 1995). It was discovered in the X–ray band as a bright, soft source during the *ROSAT* all sky survey in Dec. 1990. Further *ROSAT* observations (June 1992 to June 1993) found IC 3599 in a dimmer (~ 100) and somewhat spectrally harder state (see Fig. 1). A *Chandra* observation in March 2002 found the source at a similar level (Vaughan et al. 2004). The very large flux decrease and the softness of the X–ray spectrum led several authors to suggest that this outburst was a TDE (Brandt et al. 1995; Grupe et al. 1995; Komossa & Bade 1999; Vaughan, Edelson & Warwick 2004), even if IC 3599 is an active galaxy. Indeed active galaxies are predicted to host more TDEs due to the perturbing presence of the disc, even if it would be more difficult to reveal them because of the higher overall emission (Komossa 2012; Karas & Subr 2007). The optical spectrum is characterised by strong Hα, Hβ and [OIII] lines, showing variations in response to the X–ray outburst and classifying IC 3599 as a type 1.5-1.9 Seyfert galaxy (Brandt et al. 1995; Grupe et al. 1995; Komossa & Bade 1999). The central black hole mass has been derived from a relation between the flux at 5100 Å and the width of the quiescent Hβ emission line to be $M_\bullet^{\rm IC} \sim 3 \times 10^5 M_\odot$ (Sani et al. 2010). Grupe et al. (2015) argued that this estimate has been obtained using a Broad Line Region scaling relation, which is appropriate only in case of an unabsorbed line of sight. Using instead a black hole mass to bulge K-band luminosity (Marconi & Hunt 2003) or the relation between the [OIII] ve-

locity dispersion and the black hole mass (Nelson 2000), they found $M_\bullet^{IC}$ to be in the $(2 - 12) \times 10^6 M_\odot$ range. Here we adopt a black hole mass of $3 \times 10^6 M_\odot$. For this mass the source was well below the Eddington limit during the *ROSAT* all sky survey observation.

The (low-luminosity) AGN nature of IC3599 may cast doubts on the tidal event interpretation, because AGNs show flares, which are related to disc activity or to the uncovering of a heavily absorbed X–ray source. We note here that the quiescent *Chandra* spectrum is well described by a soft power law with minimal intrinsic absorption, weakening considerably the absorbed source case. At the same time variations by a factor of $\gtrsim 20 - 30$ in AGNs are very rarely observed. We study in details AGN variability and, based on a sample of highly variable AGNs intensively monitored by *Swift*, we can assess that a variability similar to the one observed in IC 3599 occurs by chance at $\sim 4.5\,\sigma$ level (see Appendix A). In particular, the second flare should result by chance from known AGN variability at $\gtrsim 4.0\,\sigma$. Other models apart from AGN variability, have been proposed but should not work in the case of IC 3599. A binary system made by the central black hole and an orbiting star filling its Roche lobe at periastron can be ruled out as the stellar density required would be too low (Lasota et al. 2011). In addition, we confirm that the X–ray and optical transient position is consistent with the centre of IC 3599 (see Appendix B). Periodic optical outbursts were observed in the BL Lac object OJ 287 and explained by accretion instabilities onto a binary black hole (Tanaka 2013). However, this mechanism does predict no X–rays in quiescence because the innermost part of the disc is depleted. AGN instabilities in slim disk has also been put forward to explain this variability (Honma, Matsumoto & Kato 1991). However, the estimated mass accretion rate for IC 3599 falls well below the instability region and the duration of the flares is much longer than theory predictions (Xue et al. 2011, see Appendix). All these findings lend support to the idea that IC 3599 underwent TDEs. Two different TDEs appear however unlikely. The occurrence probability of a TDE in a galaxy is of the order of 10^{-5} galaxy^{-1} yr^{-1} (e.g. Donley et al. 2002), so having two different events in 25 yr results in a probability of $\sim 6 \times 10^{-8}$. Even increasing the rate by a factor of 100 as a result of central binary black hole merger (e.g. Perets, Hopman & Alexander 2007), would result in a still low probability $\sim 6 \times 10^{-4}$. A binary disrupted by the central black hole would result into two different events but the time delay between them is way too short (several days) to account for what we observe (Mendel & Levin 2015).

IC 3599 was also detected in the radio band by the Very Large Array on June 2012. This radio observation is difficult to be accounted for challenging the prediction of the standard blast wave model (Bower et al. 2013).

4. X-ray data preparation

X–ray data were collected over a time basis of 24 years with different satellites. A log of all the observations is shown in Table 1.

4.1. ROSAT All Sky Survey data

RASS data are not straightforward to analyse. They were collected using the PSPC detector in scan mode. For this reason we decided to stick to the original analysis by Grupe et al. (1995).

4.2. ROSAT PSPC

Data were extracted using the task XSELECT (v. 2.4c) from a circular region centred on source with a 60 arcsec radius. The background spectra were extracted from an annular region centred on IC 3599, free of contaminating sources and support shadows, with inner and outer radii 125 and 250 arcsec, respectively. Data were retained in the 12–211 channel range, corresponding to an energy range of 0.1–2.4 keV. Being IC 3599 always on-axis we used the pre-canned response matrix relative to PSPC-B, gain-2 period (pspcb_gain2_256.rsp). Given the relatively low number of photons we binned the data to a minimum of one photon per energy channel using the grppha tool and adopted Cash-statistics to fit the data. Different observations were grouped together in order to increase the number of photons as indicated in Table 1.

Cash-statistics does not allow a reliable estimate of the goodness of fit. We estimate the goodness of fit by finding the best fit with Cash-statistics and then test the data with χ^2 statistics, corrected for the low number of photons per bin through the Churazov weighting scheme (Churazov et al. 1996). This allows us to determine the goodness of fit using χ^2 statistics.

4.3. ROSAT HRI

Data were first combined into a single event file using XSELECT. Source photons were extracted from a circular region of 15 arsec radius. Background photons were extracted from a nearby circular region of 45 arcsec radius. No spectral data can be obtained from *ROSAT* HRI data and the count rate was converted into a *ROSAT* PSPC count rate using PIMMS (see below).

4.4. Chandra ACIS-S

Data were reprocessed using the CIAO 4.6 (and CALDB 4.5.9) repro task. Spectral data were extracted using the CIAO task specextract using a circular 3 arcsec region for the source and an annular region for the background with 12 and 17 inner and outer radii, respectively. The task provides the user with the corresponding response matrix (rmf) and ancillary response file (arf). Data were retained in the 0.3–10 keV energy range and were binned to a minimum of one photon per energy channel using the grppha tool.

4.5. XMM-Newton Slew survey

The field of IC 3599 was observed during one XMM-Newton slew on 2007 June 19 (MJD 54270). The source was not detected with a $(2\,\sigma)$ upper limit of 0.8 counts s^{-1} in the EPIC-pn instrument (Grupe et al. 2015). This implies an upper limits on the 0.3–10 keV unabsorbed flux of 1.4×10^{-12} erg cm^{-2} s^{-1} assuming the quiescent spectral model (see below). We do not consider this observation any further.

4.6. Swift XRT

Data were reprocessed using xrtpipeline (v. 0.12.9) (CALDB 2014-07-30). Data were extracted from a circular radius of 71 arcsec and the background from a nearby circular region of 141 arcsec radius. Data were retained in the 0.3–10 keV energy range for spectroscopy and were binned to a minimum of one photon per energy channel using the grppha tool.

Table 1. IC 3599 X–ray observation log.

Instrument	Obs. ID.	Obs. start	Duration (ks)	Counts*	Spectrum
ROSAT RASS	rs931231n00	1990-12-10	0.8	–	–
ROSAT PSPC	rp700552a00	1991-12-15	3.3	101 ± 11	1
ROSAT PSPC	rp700552a01	1992-05-31	1.4	33 ± 6	2
ROSAT PSPC	rp701098n00	1992-06-16	1.8	36 ± 6	2
ROSAT PSPC	rp701099n00	1992-06-17	1.9	33 ± 6	2
ROSAT PSPC	rp701100n00	1992-06-18	2.0	36 ± 6	2
ROSAT PSPC	rp701097n00	1992-06-30	5.4	116 ± 12	3
ROSAT PSPC	rp701528n00	1993-06-17	3.4	26 ± 5	*3*
ROSAT HRI	rh702704n00	1996-06-30	14.7	77 ± 11	*3*
ROSAT HRI	rh702706n00	1996-06-30	16.9	87 ± 12	*3*
Chandra ACIS-S	acisf029999N003	2002-03-07	10.6	427 ± 21	4
Swift XRT	00037507001	2010-02-25	2.1	432 ± 23	5
Swift XRT	00037507003	2010-05-17	1.2	100 ± 11	6
Swift XRT	00037507004	2013-10-30	4.8	21 ± 6	7
Swift XRT	00037507005	2013-11-06	4.9	12 ± 4	7
Swift XRT	00037507006	2014-03-26	4.7	14 ± 4	7
Swift XRT	00037569001	2014-08-08	1.6	< 16	–
Swift XRT	00037569001	2014-11-15	4.6	18 ± 5	7
Swift XRT	00037569001	2014-11-23	0.4	< 38	–

* The total number of counts was determined using the XIMAGE (v. 4.5.1) task `detect` (correcting for vignetting and point spread function losses).

Spectra were grouped according to the scheme here reported: spectra with the same number were grouped together. Numbers in italic means that we used that given conversion factor to pass from count rates to fluxes even if no spectra analysis were carried out on these data due to the too low number of counts.

Two *ROSAT* PSPC observations on 1992-06-30 and 1992-12-08 were not considered being IC 3599 too far off-axis to be detected.
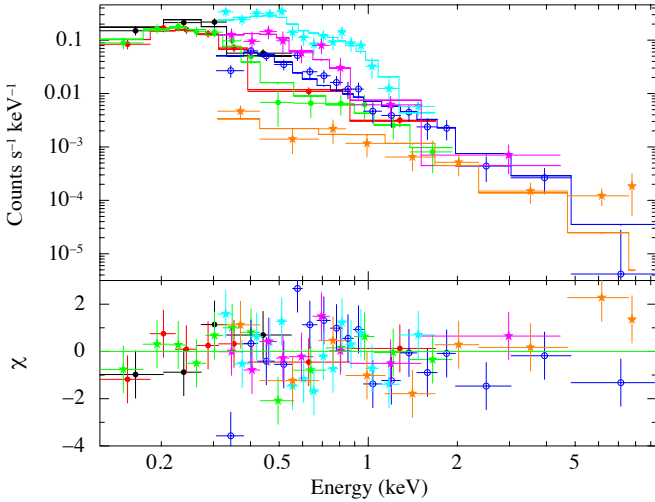

Fig. 1. X–ray spectra fitted with the absorbed disc black body plus power law model described in the text. Data were rebinned to reach a 5 σ significance or by a factor of 5 for plotting purposes only. In the upper panel black, red and green (filled circles) data refer to *ROSAT* spectra (first, second and third observations, respectively). Blue (open circles) data refer to the *Chandra* spectrum. Light blue, magenta and orange (filled stars) to *Swift* spectra (first, second and third observations, respectively). In the lower panel residuals in terms of χ are plotted with the same colour codings and symbols.

5. X–ray spectral analysis

We fitted together three *ROSAT* PSPC, one *Chandra* ACIS-S and three *Swift* XRT spectra (see Table 2) with the X–ray spectral fitting package XSPEC (v. 12.8.1g). All spectral fits were minimised using C-statistics and the goodness of the fit was assessed using the Churazov-weighted χ^2 statistics. It is readily apparent that the overall X–ray spectra are soft, as testified by previous X–ray data analysis (Brandt et al. 1995; Grupe et al. 1995; Vaughan et al. 2004). An absorbed (using TBABS) power law model with all the column densities tied together and the same photon index for all the observations returns a χ^2–statistic value of 730.9 with 410 degrees of freedom. This power law fit provides a null hypothesis probability of 10^{-20}. The power law photon index is very soft $\Gamma = 3.9 \pm 0.2$ (all errors were determined for $\Delta C = 1.0$, i.e. 1 σ errors for one parameter of interest). Leaving free the power law photon index in each spectrum improves the fit. We obtained $\chi^2 = 493.3$ with 404 degrees of freedom. The corresponding null hypothesis probability is still 0.2%. In addition, the photon index of the first *ROSAT* spectrum is extremely high with $\Gamma = 5.0^{+0.4}_{-0.4}$ and the column density $N_H = (4.4 \pm 0.1) \times 10^{20}$ cm^{-2} is much larger than the Galactic column density of $N_H = 1.2 \times 10^{20}$ cm^{-2} (Kalberla et al. 2005). A free column density model with a power law photon index fixed instead provides $\chi^2 = 619.4$ with 404 degrees of freedom, corresponding to a null hypothesis probability is 10^{-11}. A soft model such as a single black body provides similar results: $\chi^2 = 551.7$ with 404 degrees of freedom, with free temperature and radius. The null hypothesis probability is 10^{-6}. It is apparent from the fit that the black body model fails to account for a high energy tail (> 2 keV) at low fluxes.

We also considered a two component model. Given the large number of possibilities we explored two different models, based on the physics of possible emission mechanisms. The first model

comes from the proposal that this bursting activity comes from the partial disclosing of a heavily absorbed AGN. We thus model the X–ray spectra with a Galactic absorption plus a partial covering of a power law component. The second model is physically motivated by a tidal disruption event. It consists of an accretion disc spectrum (accounting for the disc emission caused by the tidal spoon-feeding) and a power law accounting for the the AGN activity (MacLeod et al. 2013).

Spectral fitting results are shown in Table 2. We explored a partial covering factor model (`pcfabs` within XSPEC) trying to see if the outburst observed in IC 3599 can be explained as the unveiling of a heavily absorbed source. This model has been envisaged to explain the wild erratic variations observed in WPVS 007 (Grupe et al. 2013). The fit is carried out with a model made by a fixed Galactic column density plus a partial covering model with the equal intrinsic column densities tied to all the spectra but variable fractions. This composite absorption component screens a power law component with the same photon index but variable normalisation. We obtained a $\chi^2 = 627.4$ for 304 degrees of freedom, resulting in a null hypothesis probability of 10^{-24} (see Table 2).

In the second model parameters are tied among different spectra. The absorbing column density is considered equal for all the spectra. The `diskbb` temperature is expected to vary, whereas its normalisation was tied between the spectra (being related to the disc inner radius and, likely, corresponding to the innermost stable orbit). The power law photon index was tied between spectra but its normalisation was free to vary. The overall fit provides a $\chi^2 = 315.9$ for 303 degrees of freedom. The null hypothesis probability is 29%. Residuals are well distributed all over the entire energy band (see Fig. 1 and Table 2). The derived column density is somewhat in excess of the Galactic value. From the normalisation of the disc black body model one can estimate the inner disc radius (modulo the disc inclination, i, and a colour factor uncertain by a factor of $f_c \sim 2$). Considering a maximally rotating black hole, we can estimate it mass as $\sim 8 \times 10^5 \times (\cos i/2)^{1/2} \times (f_c/2) M_\odot$. This estimate, even if approximate, is barely consistent with the value derived from optical studies, indicating that the central black hole in IC 3599 is not particularly massive.

Table 2. IC 3599 X–ray spectral fits.

	diskbb+pow	pcf(pow)
N_H (10^{20}) cm^{-2}	$2.8^{+0.2}_{-0.4}$	$4.4^{+1.0}_{-0.7}$
PL Γ	$2.2^{+0.2}_{-0.2}$	$3.6^{+0.1}_{-0.1}$
Diskbb norm.	1900^{+780}_{-470}	–
Dataset	T (eV)	Cov. fraction
ROS1	83^{+4}_{-12}	$0.14^{+0.07}_{-0.07}$
ROS2	75^{+4}_{-4}	$0.69^{+0.30}_{-0.02}$
ROS3	77^{+4}_{-4}	$0.95^{+0.01}_{-0.02}$
Cha1	71^{+3}_{-3}	$0.80^{+0.01}_{-0.01}$
Swi1	142^{+6}_{-7}	< 0.10
Swi2	116^{+3}_{-6}	< 0.17
Swi3	57^{+6}_{-16}	$0.98^{+0.01}_{-0.02}$
χ^2 (dof)	315.9 (303)	627.4 (304)
nhp	0.29	10^{-24}

Errors were determined with $\Delta C = 1$.

6. Light curve fitting

We fit together the luminosity light curve derived from all *Swift* X–ray data and archival *ROSAT* and *Chandra* data. To do this we computed the conversion factors from count rates to unabsorbed fluxes in the 0.01–10 keV energy band for each spectrum based on the absorbed disc plus power law spectral model. These fluxes were then converted into luminosities adopting a distance of 92 Mpc for IC 3599 and used in Fig. 2. Spectra that were obtained as the sum of different observations were then split into single observations and the same conversion factor was applied to all of them. The flux of last *ROSAT* PSPC observation was estimated based on the spectrum of the third *ROSAT* PSPC observation (i.e. the closest in time). The flux of the RASS point was extrapolated to the 0.01–10 keV energy band based on the best fit spectrum (Grupe et al. 1995). For the *ROSAT* HRI count rate we adopted a different approach. We fitted the last *ROSAT* PSPC spectrum with absorbed single component models (power law, black body and bremsstrahlung). Based on these models we used PIMMS (v. 4.7b) to extrapolate the *ROSAT* HRI rates to equivalent *ROSAT* PSPC rates. An average rate was computed and the standard deviation among the different models was added in quadrature. Then we converted these rates into fluxes as above.

The overall *Swift* light curve shows many similarities with the previous *ROSAT* light curve (Brandt et al. 1995; Grupe et al. 1995; Komossa & Bade 1999). Both bolometric light curves can be fitted with a $t^{-5/3}$ power law, pointing to (at least) two different tidal disruption events. The similarities in the decay of the events suggest that we are observing a recurrent phenomenon rather than the random occurrence of different accretion episodes. The non-disruptive passage of the same star provides a more comprehensive explanation.

We started by fitting the luminosity light curve with a different number of outbursts. Values of the χ^2 are reported in Table 3. It is readily apparent that the fit with 3 outbursts and a power law shape is superior to all the others. The improvement of a free power law index with respect to the fixed value $-5/3$ has been evaluated by means of an F-test. The probability of a random occurrence is 12%.

In addition to the luminosity light curve, we folded the temperatures derived from spectral analysis along with the suggested orbital period. Disc temperature should evolve as $T \propto t^{-5/12}$, being $\dot{M} \propto t^{-5/3}$ and $T \propto \dot{M}^{1/4}$ (from accretion disc theory, Lodato & Rossi 2010). Fitting the temperature evolution for three outburst peaks we obtain a reduced $\chi^2_{\rm red} = 0.6$ for 6 degrees of freedom and a null hypothesis probability of 75% (upper panel in Fig. 3). If we fit instead the temperature evolution for two outbursts only with the same model we derive a reduced $\chi^2_{\rm red} = 32.0$ for 6 degrees of freedom and a null hypothesis probability of 10^{-38} (orange dashed line in Fig. 3). If we add a constant to the power law model, mimicking the presence of an underlying quiescent accretion disc we obtain $\chi^2_{\rm red} = 6.6$ for 5 degrees of freedom and a null hypothesis probability of 4×10^{-6} (continuous line in the lower panel of Fig. 3). The constant quiescent disc temperature is 42 ± 6 eV. Note that such a constant temperature baseline might be present also in the first fit but it is not required by the data. We note that the presence of three peaks depends on the *Chandra* data only. If these data are strongly affected timing and spectral variability unrelated to the TDE, a longer period (twice) should be envisaged.

Based on light curve and disc temperatures evolution we found strong indication for multiple (equal) tidal stripping events. In particular, the timing and spectral data points toward three (rather than two) outbursts taking place during the 1990–
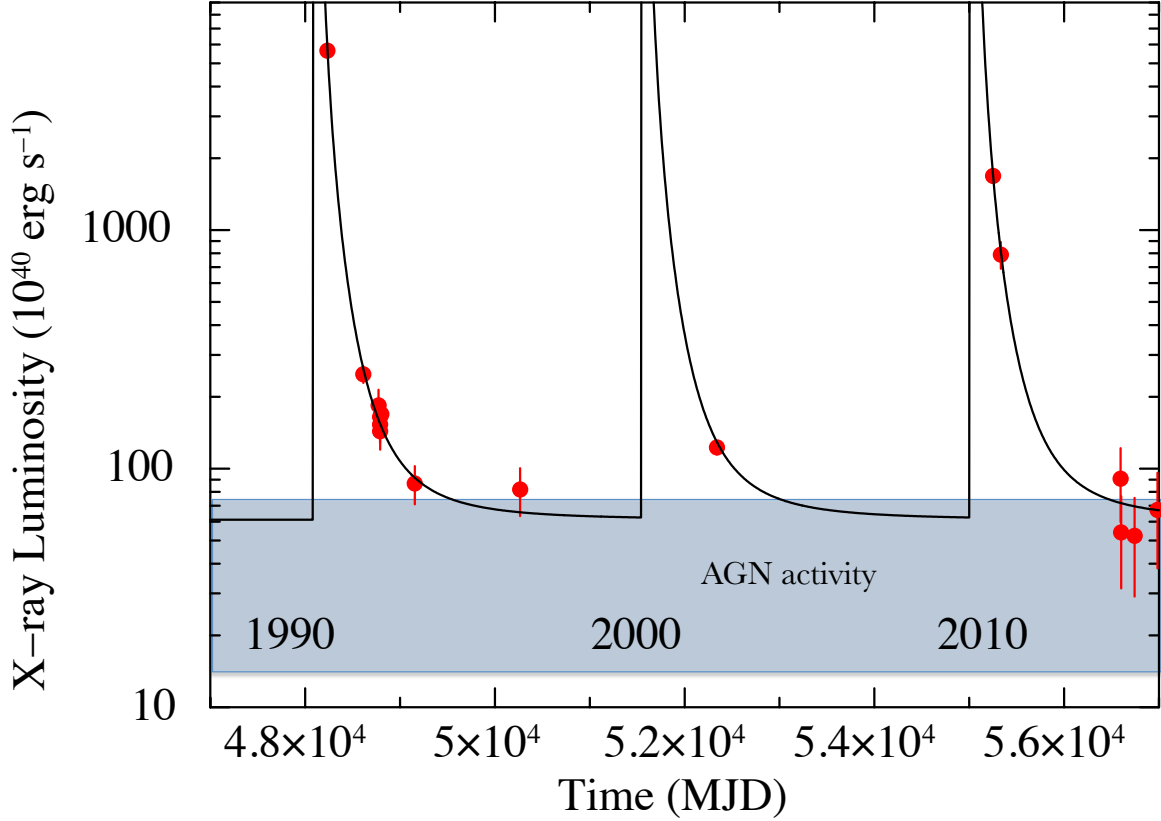
Fig. 2. Long term X–ray luminosity light curve of IC 3599. Error bars are at 1 σ confidence level. *ROSAT*, *Chandra* and *Swift* count rates were converted into 0.01–10 keV unabsorbed luminosities by means of spectral fits assuming a source distance of 92 Mpc. The overall X–ray light curve has been fit with a $(t - t_0)^{-5/3}$ function repeating over a P_0 time. Free parameters are the starting date, the power law normalisation, the repetition time and a constant, setting the basic emission level of IC 3599. The quiescent level (AGN activity) has been evaluated worsening the fit until a 10% null hypothesis probability is attained. This is nicely consistent with the mean value and the observed variability in the power law component used in the X–ray spectra fits.

Table 3. X–ray luminosity light curve fitting.

	$t^{-5/3}$ χ^2 (dof)	$t^{-5/3}$ nhp	$t^{-\alpha}$ χ^2 (dof)	$t^{-\alpha}$ nhp	α	Exp. χ^2 (dof)	Exp. nhp	$e-$ fold (d)
2 outburst	37.3 (12)	2×10^{-4}	25.3 (11)	8×10^{-3}	-3.8 ± 1.2	33.0 (11)	5×10^{-4}	108 ± 9
3 outburst	9.3 (12)	7×10^{-1}	7.1 (11)	8×10^{-1}	-2.7 ± 1.1	28.4 (11)	3×10^{-3}	112 ± 6
4 outburst	29.0 (12)	4×10^{-3}	24.3 (11)	1×10^{-2}	-3.6 ± 1.6	33.0 (11)	5×10^{-4}	108 ± 6

2014 time span, with a recurrence time of 9.5 yr (see Figs. 2 and 3). Assuming an accretion efficiency of $\eta = 0.1$, from the outburst light curve we can estimate the peak mass accretion rate to be $\dot{M}_{\mathrm{peak}} \sim 0.01 M_\odot$ yr^{-1} and the accreted mass per episode to be $\Delta M \sim 2.5 \times 10^{-3} M_\odot$. Clearly these are lower limits, missing the early stages of all the outbursts. In addition, with these new ephemerides, radio observations took place only 2.6 yr after an outburst episode and can be accounted for by emission internal to the jet (van Velzen, Körding & Falcke 2011).

7. Optical data

IC 3599 fell within the field of view of the Catalina sky survey and was monitored in the optical in the MJD 53470–56463 interval (Drake et al. 2009). The Catalina light curve shows a broad peak (see Fig. 4). The light curve can be fit with a Gaussian centred on MJD 55151 ± 11 (1 σ) and with width of 200 ± 18 d. The peak of the optical emission occurs after the estimated peak of the X–ray emission by ~ 140 d. However, due to the large width of the optical flare, the optical emission starts ~ 280 d before the high energy peak (assuming as the start of the optical flare when the optical flux rises by 10% over the constant value).
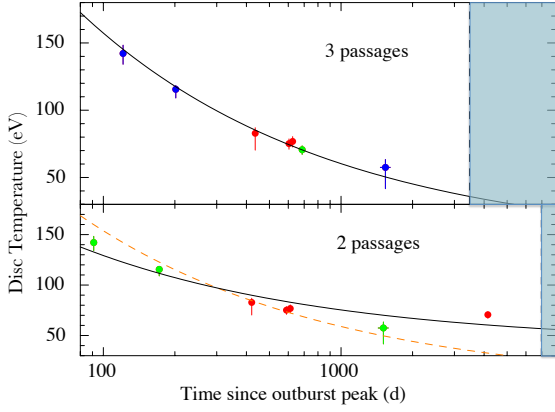
6

Fig. 3. *Upper panel*: disc temperatures as derived from the spectral fits folded on a three passages light curve. Error bars are at 1σ confidence level. Red points (*ROSAT*) refer to the first passage, the green point (*Chandra*) to the second passage and blue points (*Swift*) to the third one. Disc temperature evolution is fitted with a fixed $T \propto t^{-5/12}$ power law (deriving from $\dot{M} \propto t^{-5/3}$ and $T \propto \dot{M}^{1/4}$ typical of an accretion disc and therefore being a direct test for the disc cooling, Lodato & Rossi 2010). *Lower panel*: as above but in the case of two passages. Red dots (*ROSAT* and *Chandra*) refer to the first passage and green dots (*Swift*) to the second one. The fit with a $T \propto t^{-5/12}$ power law is shown as a dashed orange line.

This gives us the possibility to study in detail the outburst start (and prepare a follow-up strategy for the next outburst). The rise time in a TDE is governed by the circularisation time (i.e. the time to form the accretion disc) and the viscous time (i.e. the time needed to transfer matter from the outer disc edge to the central compact source). Several papers have appeared recently on this subject (Bonnerot et al. 2015; Guillochon & Ramirez-Ruiz 2015; Piran et al. 2015). Irrespective of which is the dominant mechanism, we can safely assume that the viscous time of the disc, t_ν, is shorter than the observed rise time. Given the optical light curve the time it takes to rise from 10% of the quiescent flux to the peak flux is ~ 420 d. Fitting the optical light curve with a symmetric exponential function, we derive an e−folding rise/decay time of 178 ± 14 d. Based on Guillochon & Ramirez Ruiz (2013), the viscous time can be expressed as:

$$t_\nu = 12\,\beta^{-3}\,M_*^{-1/2}\,R_*^{3/2}\,\alpha_{0.1}^{-1}\ \text{d}$$

8. Constraining the orbit and star characteristics

Partial disruption of stars has been investigated by means of hydrodynamical simulations (Guillochon & Ramirez Ruiz 2013; Macleod et al. 2013; Macleod et al. 2012). Depending on the star structure (modelled as a polytrope with index $\gamma = 4/3$ or $5/3$), it has been shown that mass can be extracted from the star for impact parameter β as low as 0.5–0.6 whereas complete destruction occurs for $\beta > 0.90$ for $\gamma = 5/3$ and for $\beta > 1.85$ for $\gamma = 4/3$, respectively (Guillochon & Ramirez Ruiz 2013). In order to constrain the encounter and star characteristics we compare the mass accretion at peak rate $\dot{M}_{\text{peak}}$ and the total amount of matter $2\,\Delta M$ lost by the star during each passage with the corresponding quantities estimated through hydrodynamical simu-
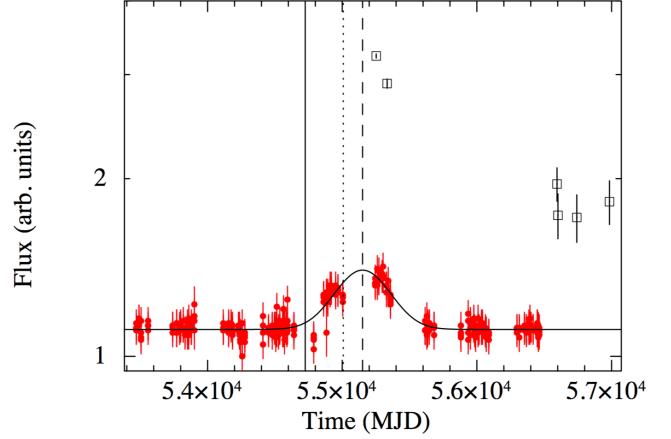

Fig. 4. Optical (flux) light curve of IC 3599 from the Catilina sky survey in arbitrary units (red dots), together with the *Swift*/XRT light curve (open squares) converted in flux using the spectral fit model, in arbitrary units. The Gaussian fit refers to the optical data. The vertical dashed line marks the time (MJD) of the optical peak, the dotted line the peak of the X–ray flux according to the multi-peak modelling. The continuous line marks the time at which the optical light curve rises by 10% from the quiescent level.

lations (Guillochon & Ramirez Ruiz 2013). These quantities depend strongly on the impact parameter β and, to a lesser extent, on the star mass and radius.

The peak mass accretion rate has been estimated based on the RASS data, converting the peak luminosity into a peak mass accretion rate by assuming a 10% conversion efficiency. In order to bracket uncertainties the allowed parameter space is computed accepting values of the peak accretion rate in the interval 1–3 of observed value. The other parameter considered is the total amount of mass accreted during one flare episode. This has been estimated by integrating the luminosity light curve over one orbital period. Also for this parameter we searched solutions in the interval 1–3 of the observed total mass accreted. Finally, we require that the viscous time of the disc, t_ν, is shorter than 178 ± 42 d (3σ). A mass range of $0.2 - 100 M_\odot$ and a (unrelated) radius range of $0.01 - 10^4 R_\odot$ were blindly searched. We consider two different star models based on a polytropic index of $\gamma = 4/3$ (over the interval $\beta = 0.5 - 4.0$) and $\gamma = 5/3$ ($\beta = 0.45 - 2.5$). Results are shown in Fig. 4 for the two indexes separately.

In case of $\gamma = 4/3$ we find solutions in the range $\beta = 0.58 - 0.72$. The range of allowed values of β has been obtained without requiring a priori a partial disruption event, searching for solution in the $\beta = 0.5 - 4.0$ interval. This results therefore strongly (and independently) supports that the flaring events in IC 3599 are related to a partial tidal disruption ($\beta < \beta_c = 1.85$) of an orbiting star. The corresponding mass range is for $M_* > 4M_\odot$. We blindly explored the mass-radius plane, but stars do not fill this plane homogeneously. To test the consistency of our findings with stellar models, we investigated the mass-radius relation by means of the Single Stellar Evolution (SSE) code (Hurley, Pols & Tout 2000), assuming solar metallicity (we verified that a change in the metallicity does not change our results sensibly). With this additional constraint we have that the range of allowed masses reduces to $M_* = 15 - 45 M_\odot$ for stars on the main sequence and to $M_* = 4 - 15 M_\odot$ for slightly evolved stars. The corresponding radii in the selected region are $R_* \sim 5 - 9 R_\odot$

for main sequence stars and $R_* \sim 4 - 7 R_\odot$ for slightly evolved stars (see Fig. 4 upper panel). The allowed eccentricities range in $e \sim 0.995 - 0.997$ and the pericentre distance $r_p \sim 84 - 93 r_g$ (where $r_g = G M_\bullet^{IC}/c^2$ is the gravitational radius of the black hole in IC 3599, G the gravitational constant and c the speed of light). The eccentricity is high but not unlikely given the predicted distribution of eccentricities around the central black hole in our Galaxy (Gillessen et al. 2009). This eccentricity is larger than the critical eccentricity for bound orbits below which all stellar debris remains bound and feed the black hole on a longer time scale (Hayasaki et al. 2013).

In the case of a polytropic star with index $\gamma = 5/3$, we searched solutions for β in the 0.45–2.5 range (see Fig. 4 lower panel). We do find solutions in a narrow range of $\beta = 0.49 - 0.55$. Again the allowed range of β is well below the critical value for a complete tidal disruption ($\beta_c = 0.9$). The allowed mass range is $M_* \gtrsim 1.5 M_\odot$. However polytropic stars with $\gamma = 5/3$, can satisfactorily describe Sun-like stars (or smaller) and we do not find therefore acceptable solutions in this case.

9. Conclusions

We report here on the first candidate of periodic, partial tidal disruption events. These events were observed as large (> 100) flux increases in the 24-yr long X–ray light curve of the close, low-luminosity active nucleus IC 3599 (see Fig. 2). We discuss several possibilities to explain these large flares and likely conclude that they cannot be ascribed to AGN variability: single flares are unlikely, at $\gtrsim 4.0\,\sigma$ level, to come from known, observed extremely variable AGNs, and the flaring instability region suggested by some accretion disc models (e.g. Honma et al. 1991) lies above the mean accretion rate observed in IC 3599 by a factor of $\gtrsim 15$. By modelling the light curve and the disc temperature evolution, as derived by spectral fits, we find out that three flares are statistically preferable over two, resulting in a ~ 9.5 yr periodicity. This cannot be appreciated from the light curve where the second flare is largely missed due to sparse observations, but results from the disc temperature evolution: if the standard disc model can apply to the observations of IC 3599, then the 3-outbursts model is preferable over the 2-outburst model at $\sim 3.8\,\sigma$. Based on the disc temperature evolution the same is true at $\sim 4.3\,\sigma$ confidence level. A tidal disruption model applied to IC 3599 provides a good match to the data and, independently, solutions for partial disruption events only.

In addition, we note that the average quiescent luminosity of the AGN is just a fraction of average flare luminosity ($\sim 20\%$), leaving open the possibility that the overall AGN activity of IC 3599 is entirely spoon-fed by the orbiting star (MacLeod et al. 2013). Given the relatively large mass stripped every passage, the phenomenon is short-lived and based on our estimates it can last $\lesssim 10^4$ yr. The next passage should occur in 2019, giving us the ability to plan a detailed monitoring campaign to explore the characteristics of the orbiting star. The very short orbital period gave us the possibility to observe more than one passage. Other tidal disruption events presently known might be similar to this case but just with a longer orbital period.

References

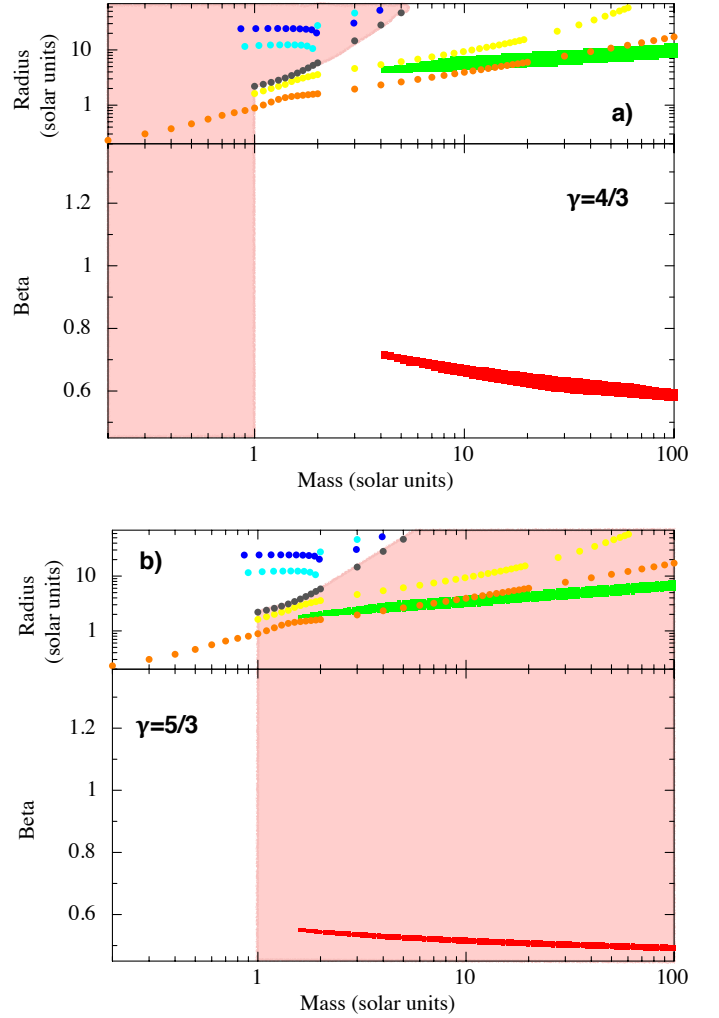Abramowicz, M. A., Czerny, B., Lasota, J. P., Szuszkiewicz, E. 1988, ApJ, 332, 646

Fig. 5. Radius of the orbiting star and impact parameter $\beta = r_t/r_p$ as a function of the star mass. The allowed regions were computed based on fitting formulae in Guillochon & Ramirez-Ruiz (2013 and related errata corrige). *Upper panel*: orbiting stars characterised by a polytropic index $\gamma = 4/3$. The red region in the lower panel shows the allowed β parameters. The light red region approximately exclude the low mass end ($\lesssim 1 M_\odot$) and the stars more evolved than the giant branch because they are not well described by a polytropic index $\gamma = 4/3$. Orange dots indicate stars in the main sequence phase, yellow dots the Hertzsprung gap, black dots the giant branch, light blue dots the helium core-burning, and blue dots the asymptotic giant branch phase. *Lower panel*: shows the case of a polytropic star with index $\gamma = 5/3$. Colours, dots, and regions are as above. The light red region approximately excludes the high mass end ($\gtrsim 1 M_\odot$), because these stars are not well described by a polytropic index $\gamma = 5/3$ (but includes evolved giant stars). No acceptable solutions remain for this case.

Bloom, J. S. , et al. 2011, Sci, 333, 203
Bonnerot, C., et al. 2015, MNRAS submitted (arXiv :1501.04635)
Bower, C. B., Metzger, B. D., Cenko, S. B., Silverman, J. M., Bloom, J. S. 2013, AJ, 763, 84
Brandt, W. N., Pounds, K. A., Fink, H. 1995, MNRAS, 273, L47
Breeveld, A. A., Landsman, W., Holland, S. T., Roming, P. , Kuin, N. P. M., Page, M. J. 2011, AIPC, 1358, 373
Burrows, D. N., et al. 2011, Nat, 476, 421
Cenko, S. B., et al. 2012, ApJ, 753, 77

Churazov, E., Gilfanov, M., Forman, W., Jones, C. 1996, ApJ 471, 673
Donley, J. L. , Brandt, W. N., Eracleous, E. Boller, Th. 2002, AJ, 124, 1308
Drake, A. J., et al. 2009, ApJ, 696, 870
Evans, C. R., Kochanek, C. S. 1989, ApJ, 346, L13
Gezari, S. 2012, EPJWC, 39, 3001
Gezari, S., et al. 2012, Nat, 485, 217
Gillessen, S., Eisenhauer, F., Trippe, S., Alexander, T., Genzel, R., Martins, F., Ott, T. 2009, ApJ, 692, 1075
Gillessen, S., et al. 2012, Nat, 481, 51
Grupe, D., Komossa, S., Leighly, K. M. , Gallo, L. C. 2012, EPJWC, 39, 6001
Grupe, D., Thomas, H.-C., Beuermann, K. 2001, A&A, 367, 470
Grupe, D., Thomas, H.-C., Leighly, K. M. 1999, A&A, 350, L31
Grupe, D., et al. 1995, A&A, 299, L5
Grupe, D., et al. 2013, AJ, 146, 78
Grupe, D., Komossa, S., Saxton, R. 2015, ApJ, 803, L28
Guillochon, J., Loeb, A., MacLeod, M., Ramirez-Ruiz, E. 2014, ApJ, 786, L12
Guillochon, J. Ramirez-Ruiz, E. 2013, ApJ 767, 25
Guillochon, J. Ramirez-Ruiz, E. 2015, ApJ submitted (arXiv:1501.05306)
Hayasaki, K., Stone, N., Loeb, A. 2013, MNRAS 434, 909
Hirose, S., Krolik, J. H., Blaes, O, 2009, ApJ, 691, 16
Ho, L. C. 2008, ARA&, 46, 475
Honma, F., Matsumoto, R., Kato, S. 1999, PASJ, 43, 147
Hopkins, P. F., et al. 2006, ApJS, 163, 1
Hurley, J. R., Pols, O. R., Tout, C. A. 2000, MNRAS, 315, 543
Ivanov, P. B., Novikov, I. D. 2001, ApJ, 549, 467
Kalberla, P. M. W. , et al. 2005, A&A, 440, 775
Karas, V., Subr, L. 2007, A&A, 470, 11
Komossa, S., Bade, N. 1999, A&A, 343, 775
Komossa, S. 2012, EPJWC, 39, 2001
Lacy, J. H., Townes, C. H., Hollenbach, D. J. 1982, ApJ, 262, 120
Lasota, J.-P., et al. 2011, ApJ, 735, 89
Lodato, G., King, A. R., Pringle, J. E. 2009, MNRAS, 392, 332
Lodato, G., Rossi, E. M. 2010, MNRAS, 476, 359
MacLeod, M., Ramirez-Ruiz, E., Grady, S., Guillochon, J. 2013, ApJ, 777, 133
MacLeod, M. Ramirez-Ruiz, E. Guillochon, J. 2012, ApJ, 757, 134
Marconi, A., Hunt, L. 2003, ApJ, 589, L21
McHardy, I. M., Koerding, E., Knigge, C. Uttley, P, Fender, R. P. 2006, Nat, 444, 730
McHardy, I. M., Papadakis, I. E., Uttley, P, Page, M. J., Mason, K. O. 2004, MNRAS, 348, 783
Mendel, I., Levin, Y. 2015, ApJ, 805, L4
Nelson, C. H. 2000, ApJ, 544, 91
Perets, H. B., Hopman, C., Alexander, T. 2007, ApJ, 656, 709
Phinney, E. S. 1989, in Proc. 136th IAU Symp. 'The Center of the Galaxy'
Piran, T., et al. 2015, ApJ submitted (arXiv:1502.05792)
Poole, T. S., et al. 2008, MNRAS, 383, 627
Rees, M. J. 1988, Nat, 333, 523
Renzini, A., et al. 1995, Nat, 378, 39
Sani, E., et al. 2010, MNRAS, 403, 1246
Saxton, R. D., et al. 2014, A&A, 572, A1
Shappee, B. J., et al. 2014, ApJ, 788, 48
Strubbe, L. E., Quataert, E. 2009, MNRAS, 400, 2070
Tanaka, T. L. 2013, MNRAS, 434, 2275
Ulmer, A. 1999, ApJ, 514, 180
van Velzen, S. Körding, E. Falcke, H. 2011, MNRAS, 417, L51
Vaughan, S., Edelson, R., Warwick, R. S. 2004, MNRAS, 349, L1
Vaughan, S., Edelson, R., Warwick, R. S., Uttley, P. 2003, MNRAS, 345, 1271
Xue, L., Sadowski, A., Abramowicz, M. A., Lu, J.-F. 2011, ApJS, 195, 7

Appendix A: AGN variability

Given the low-luminosity AGN nature of IC 3599 we investigated in details here if the observed flares can come from this activity. We approached the problem either studying standard AGN variability and by taking an unbiased sample of the most variable AGNs as observed by the *Swift* satellite.

A.1. Intrinsic AGN variability

We simulated the long-term light curve of an AGN (Vaughan et al. 2003). We assumed a standard broken power law for the power spectral density (PSD) of a long term (years) monitoring light curve. We considered an index −1 at short frequencies and −2 at high frequencies, with a break at 10^3 Hz scaled to the mass and luminosity of the black hole in IC 3599 (McHardy et al. 2006). We checked that even heavily changing these numbers the final result does not depend on them. We run a simulation generating a number of light curves based on the PSD above, including no root-mean-square (rms) variability and no background. The long-term light curve changes in all cases are less than a factor of a few with respect to the mean starting value (on timescales of days). We then turned on the rms variability and this value is the main driver for the variability. Even assuming a 100% rms variability, we obtained a maximum increase by a factor of $\sim 6 - 7$ in the count rates (no background included) from the mean value on timescales longer than days. From this analysis we conclude that normal AGN variability is not able to produce the strong variability we observe.

A.2. AGN with large intrinsic variations

We started from *Swift*/XRT light curves spanning a 10 yr basis. We first considered the AGN sample monitored by BAT, consisting of bright nearby AGNs with more than 5 *Swift*/XRT observations. In this sample there are just 3 AGNs showing a count rate change by more than a factor of 20. These are Mkn 335 ($\Delta = 42$), NGC 4395 ($\Delta = 141$) and CGCG 229–015 ($\Delta = 56$, even if in this case the change is a dip rather than a flare). One very efficient method to find highly variable AGN consists in comparing soft X–ray observations at different epochs. Grupe et al. (2001) showed that 4 out of 113 bright RASS objects observed also in ROSAT pointings showed dramatic variations. Grupe et al. (2012) added other 4 objects to this list by means of subsequent *XMM-Newton* and *Chandra* observations. All but two are Narrow Line Seyfert 1 galaxies. The first is RX J1624.9+7554, a non-active galaxy for which a TDE has been invoked (Grupe et al. 1999), the second one is IC 3599. In this Grupe-Komossa sample of highly variable AGNs there are then 8 objects but only 3 of them show variations larger than a factor of 30. These are 1H 0707–495 ($\Delta = 114$, dip-like variation), Mkn 335 (as above) and WPVS 007 ($\Delta = 36$). WPVS 007 is however too faint for Swift and the light curve is unusable because it has too few points (Grupe et al. 2013). We have then 4 objects with good-enough sampled light curves, showing flare-like features (Fig. A.1).

One conservative test is to extract randomly from these curves 7 points (the number of points comprising the first TDE flare) and 6 points (the number of points comprising the third TDE flare) separately, and fit them with a tidal decay template $(t - t_0)^{5/3} + c$ to mimic one TDE at a time. We simulated 500,000 light curve realisations for each source by randomly sampling the observed light curves, extracting 7 or 6 points, respectively. We then excluded simulated light curves with a rate variation less than a factor of 30 (in order not to fit constants, note that even if the flux variation in the *Swift*/XRT data is ~ 30 the count rate variation is ~ 100 due to spectral variability, therefore our rate change provides a conservative estimate) and fit the remaining light curves with the above model. We adopted two different approaches. In the first one we counted how many simulations have a null hypothesis probability larger than 5% and, based on this number, evaluated the probability of obtaining by chance a TDE-like light curve. In the second approach we took among all these light curves the best one in terms of χ^2 and derived the probability of this χ^2 with respect to the number of degrees of freedom (5 and 4 in our case, respectively). We do this because even the best selected χ^2 is, for some sources, not good, at variance with the fit of the IC 3599 flare. This χ^2 probability is then weighted for the number of trials (500,000). With these numbers we assessed the probability of randomly extract a TDE-like
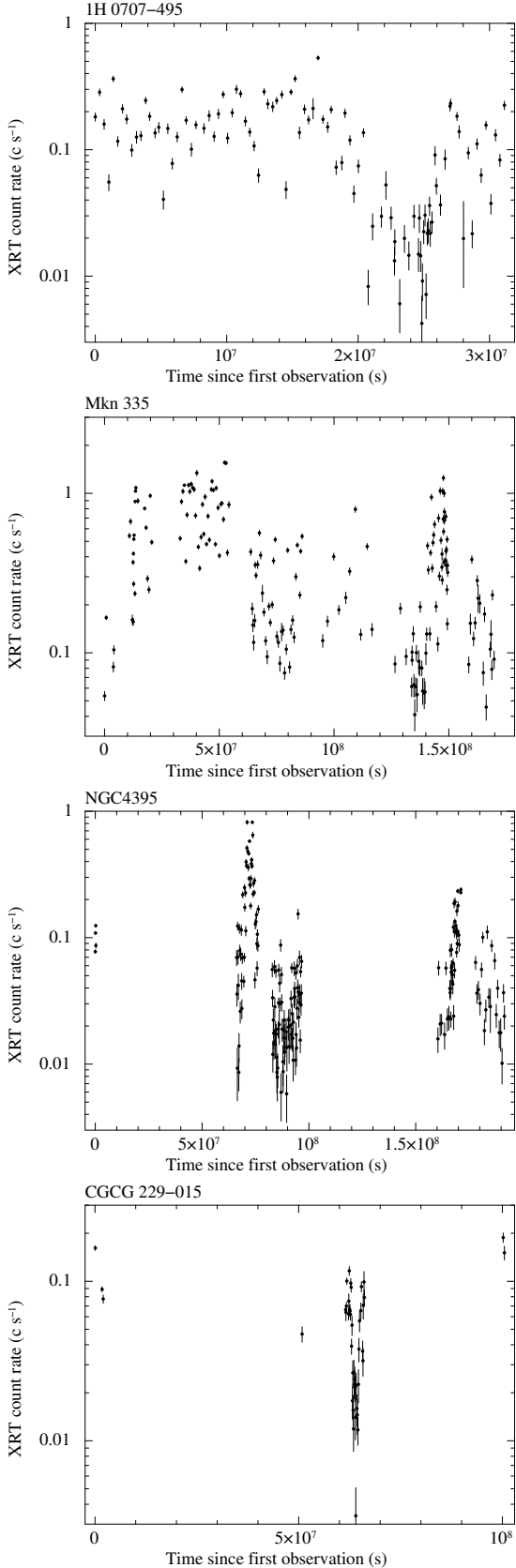
Fig. A.1. *Swift*/XRT light curves of the 4 selected highly variable AGN.

tor of > 30 (the *Swift* rate variation is ~ 100). We obtained in this way conservative limits that are shown in Table A.1.

A different check can be made on the spectral properties of IC 3599. In Fig. A.2 we show the spectral evolution of the five sources in our sample. This is quantified in terms of hardness ratio (computed as $HR = (H - S)/(H + S)$, being H and S the counts in the 2–10 keV and 0.5–2 keV energy bands, respectively, so that HR can vary among −1 and 1) versus cont rates normalised to the minimum observed rate. In this plane IC 3599 stands alone, reaching complete softness ($HR = -1$) at maximum and showing a clear spectral evolution. 1H 0707–495 is similarly soft but it does not show a marked spectral variability as the count rate changes. Mkn 355 and NGC 4395 show spectral marked changes but never appear as very soft sources.

We should safely conclude that the flares observed in IC 3599 do not likely come from known (observed) AGN variability.
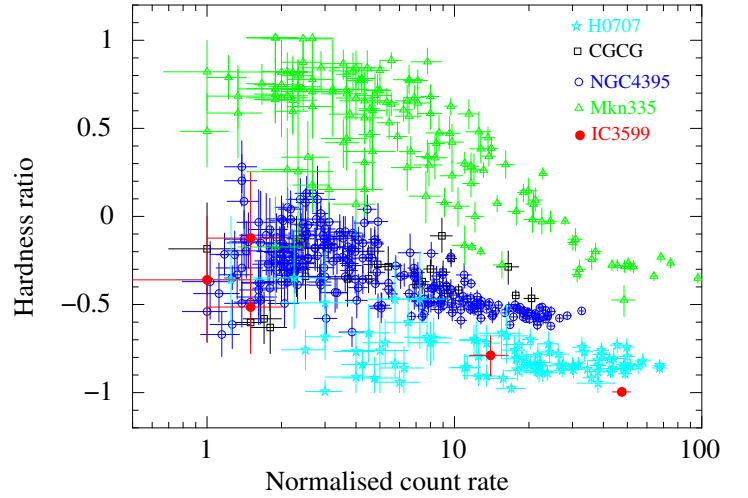

Fig. A.2. Hardness ratio as a function of the normalised count rates for the variable AGNs described above. 1H 0707–495 data are shown as light blue open stars, CGCG 229–015 as black open squares, NGC 4395 as blue open circles, Mkn 335 as green open triangles, and IC 3599 as filled red circles. Count rates are normalised to the minimum rate observed. The hardness ratio is computed as the ratio as $(H - S)/(H + S)$ being H the number of counts in the 2–10 keV energy band and S those in the 0.5–2 keV band.

A.3. Disk instability models

The standard geometrically thin, optically thick accretion disc model has thermally unstable regions if the accretion rate is larger than a critical value. A new branch of equilibrium solutions should exist for rate across the Eddington luminosity, named slim discs (Abramowicz et al. 1988). Some works have shown that a limit cycle might take place, resulting in a flare-like behaviour (Honma et al. 1991). Magneto-Hydrodynamical simulations showed, on the contrary, that such disks could be thermally stable (Hirose, Krolik & Blaes 2009). Observationally, Galactic transient X–ray binaries in outburst do not show any evidence for such an instability, except perhaps GRS 1915+105 (Xue et al. 2011).

The mean mass accretion rate of IC 3599 is ~ 0.005 in Eddington units (for an efficiency of 10%, where the peak accretion rate reaches ~ 0.1 the Eddington rate), far away from

event from these light curves with a count rate increase by a fac-

Table A.1. Simulated light curves from Swift/XRT variable AGN searching for random TDE-like events.

Source	TDE1 probab. (σ)	TDE3 probab. (σ)	Num. Obs.	Variation	Type
1H 0707–495	4.11(4.95)	4.06(4.84)	101	$\Delta = 114$	dip
Mkn 335	> 4.75(7.93)	> 4.75(7.89)	179	$\Delta = 42$	flare
NGC 4395	> 4.75(5.74)	4.06(4.94)	190	$\Delta = 141$	flare
CGCG 229–015	> 4.75(> 8.31)	> 4.75(> 8.31)	44	$\Delta = 56$	dip

Probability of the first and third IC 3599 flares to be obtained by sampling the *Swift*/XRT light curves of highly variable AGNs. The first probability is obtained by requiring that the simulated light curve has a null hypothesis probability larger than 5%. The second probability (in parenthesis) is obtained by weighing the best fit light curve probability with the number of simulations carried out.

border of the unstable region, starting at a critical mass accretion rate > 0.1 in Eddington units (Honma et al. 1991). Flare models do not make a clear prediction of the shape of the flare but make key prediction that the flare width is a very short fraction of the times between two different flares (Xue et al. 2011). The ratio of the FWHM of the flare with respect to the duration time between two consecutive flares must be $\lesssim 3.6\%$. We modelled the two main peaks of IC 5399 with a Gaussian, limiting the maximum luminosity to a few times the Eddington value, and found a FWHM~ 500 d (leaving free the maximum luminosity provides a better fit and an even larger FWHM~ 1200 d). Taking the times among the two main flares, we obtain a ratio of ~ 7% (~ 17% for a free Gaussian shape). This is more than double what expected based on models.

We also note that two possible very recent flare-like events in AGNs, XMM SL1 J061927.1–655311 (Saxton et al. 2014) and NGC 2617 (Shappee et al. 2014), involve smaller flux variations ($\lesssim 20$) and much more complicated X–ray light curves.

Appendix B: UVOT analysis

B.1. Image analysis

Together with XRT exposure, the *Swift* satellite took contemporaneous images of IC 3599 with the UVOT instrument. During all the six *Swift* observations (but the fourth), UVOT observed IC 3599 with all its 6 filters (in the fourth only with the uvm2 filter). Sky images were considered and fluxes were obtained with the `uvotsource` task using the latest calibrations (Poole et al. 2008; Breeveld et al. 2011). For UV images a circular extraction region of 8 arcsec radius has been considered and for optical image a 5 arcsec radius, respectively. A background region close to IC 3599 free of sources and of 20 arcsec radius has been selected. Results are shown in Table B.1. A clear decrease in flux is apparent, especially at UV wavelengths with a decrease by a factor of ~ 2 (uvm2).

B.2. Astrometry

In order to determine precisely the position of the transient source observed in IC 3599, we carried out digital image subtraction between the first and the last UV frames (uvm2) obtained with the Swift/UVOT. In the first image, obtained on 2010 February 25, the transient source is at its maximum while in the last epoch, obtained on 2014 March 26, it has faded below the host galaxy level (Table B.1). Both images were obtained with the uvm2 filter and have exposure times of 0.2 ks and 1.2 ks, respectively. Before subtraction, the two images were aligned. We accounted for the difference in the exposure times by multiplying the image obtained on Feb 2010 by a factor of six. As can be seen in the third panel of Fig. B.1, the result of the im-

Table B.1. IC 3599 UVOT data analysis.

Time (MJD)	Flux 10^{-15} erg cm^{-2} s^{-1} Å^{-1}
v band	(5468 Å)
55252.3	2.23 ± 0.11
55333.0	2.00 ± 0.09
56594.9	1.70 ± 0.10
56741.9	1.61 ± 0.08
b band	(4392 Å)
55252.3	2.20 ± 0.09
55333.0	2.03 ± 0.07
56594.9	1.63 ± 0.08
56741.9	1.58 ± 0.06
u band	(3465 Å)
55252.3	1.97 ± 0.08
55333.0	1.79 ± 0.07
56594.9	0.99 ± 0.06
56741.9	1.03 ± 0.05
uvw1 band	(2600 Å)
55252.3	2.43 ± 0.10
55333.0	2.20 ± 0.08
56594.9	1.09 ± 0.06
56741.9	1.19 ± 0.06
uvm2 band	(2246 Å)
55252.3	2.59 ± 0.12
55333.0	2.55 ± 0.11
56594.9	1.16 ± 0.08
56601.9	1.22 ± 0.04
56741.9	1.23 ± 0.04
uvw2 band	(1928 Å)
55252.3	2.90 ± 0.09
55333.0	2.71 ± 0.08
56594.9	1.43 ± 0.06
56741.9	1.33 ± 0.05

Errors are at $1\,\sigma$ confidence level.

age subtraction is good, showing a clear residual at the position of IC 3599. The position of this residual is RA, Dec (J2000): 12:37:41.18, +26:42:27.0 (with an uncertainty of 0.3 arcsec, calibrated against the USNOB1.0 catalogue). At the distance of IC 3599 1 arcsec corresponds to 0.4 kpc. The residual is located at 0.8 ± 0.4 arcsec ($1\,\sigma$ confidence level) with respect to the position of the IC 3599 galaxy centre and is fully consistent with the position of the candidate TDE radio counterpart (Bower et al. 2013). The consistency of the position of the UV transient with the IC 3599 galaxy centre (at the $2\,\sigma$ level) is in agreement with a TDE origin.
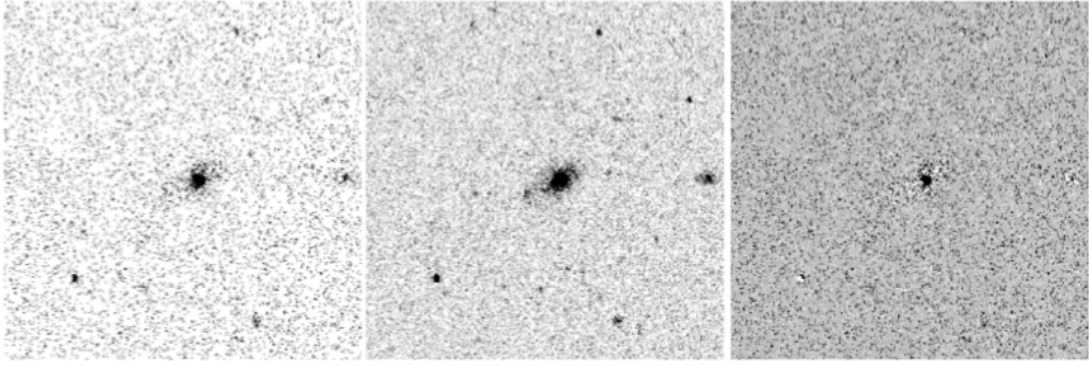
Fig. B.1. Swift/UVOT images of IC 3599, obtained with the uvm2 filter on 2010 Feb 25 (left panel) and 2014 March 26 (central panel). The images are $5' \times 5'$, North is up, East is left. The right panel shows the result of digital image subtraction between these two images. A clear residual is visible at a position consistent with the IC 3599 galaxy centre.